Self-Consistent Polarization Density Functional Theory: Application to Argon†

Katie A. Maerzke,‡ Garold Murdachaew,§ Christopher J. Mundy,*,§ Gregory K. Schenter,*,§ and J. Ilja Siepmann‡

Department of Chemistry and Department of Chemical Engineering and Materials Science, University of Minnesota, Minneapolis, Minnesota 55455, and Chemical & Materials Sciences Division, Pacific Northwest National Laboratory, Richland, Washington 99352

Received: October 3, 2008; Revised Manuscript Received: December 3, 2008

We present a comprehensive set of results for argon, a case study in weak interactions, using the self-consistent polarization density functional theory (SCP-DFT). With minimal parametrization, SCP-DFT is found to give excellent results for the dimer interaction energy, the second virial coefficient, the liquid structure, and the lattice constant and cohesion energy of the face-centered cubic crystal compared to both accurate theoretical and experimental benchmarks. Thus, SCP-DFT holds promise as a fast, efficient, and accurate method for performing *ab initio* dynamics that include additional polarization and dispersion interactions for large, complex systems involving solvation and bond breaking.

1. Introduction

Accurately describing chemical reactions in the condensed phase remains a significant challenge for molecular simulations, requiring the explicit and computationally expensive treatment of the electrons via a quantum mechanical theory. One popular theory that provides a compromise between speed and accuracy is Kohn−Sham (KS) density functional theory (DFT),[1,2] which is widely used and implemented in many available software packages. While DFT is in principle exact, a significant deficiency of the current DFT exchange-correlation (XC) functionals is that they are of either local character (local density approximation, or LDA) or of semilocal character (generalized-gradient approximation, or GGA, with an additional dependence on density gradients). These functionals, requiring charge overlap to result in an interaction, cannot recover the long-range correlation needed to represent the dispersion component which is present even at distances where charge overlap may be negligible.[3] Even the newer meta-GGA functionals (with additional dependence on the kinetic-energy density and/or the Laplacian of the density, i.e., TPSS)[4] are still only semilocal. Thus, standard DFT cannot accurately model weak interactions.[5,6] However, since DFT is essentially parameter free, it holds tremendous promise for describing complex chemical phenomena in hydrogen-bonding fluids where dispersion effects are less important. Examples include simulations exploring different sampling strategies in first-principles simulations of water,[7] the liquid−vapor interface of methanol,[8] benzene solvated in water,[9] and the confinement of water within nanotubes and between graphene sheets.[10] Given the failure of present day XC functionals to capture subtle weak interactions that are known to be present in the aforementioned systems, one must conclude that any good agreement with experiment or more accurate calculations for weakly bound systems is likely to be accidental. On a positive note, DFT-GGA, by its good description of the molecular electronic density and multipole moments, seems to perform reasonably well for hydrogen-bonded systems such as water near its minimum configurations[5,6] in which the first-order electrostatic interactions are dominant. Thus, systems in which extensive hydrogen-bonded networks are formed may be relatively well-represented by DFT XC functionals such as BLYP or PBE,[5,6,11] but neither performs satisfactorily for the vapor−liquid coexistence curve of water.[12,13]

The proper description of weak interactions requires a wave function based theory and a careful treatment of the electron correlation. Thus, with a supermolecular approach,[14] one must use MP2 (Möller−Plesset method of second order) or, much better, CCSD(T) (coupled-cluster expansion including single, double, and noniterated triple excitations), the most accurate of readily available and affordable supermolecular methods, at least for generating potential energy surfaces (PESs) for small- and medium-size systems (see, for example, Bukowski et al.[15]). Yet another robust approach for studying weakly bound systems is symmetry-adapted perturbation theory of intermolecular interactions, or SAPT,[16] and its more efficient variant, SAPT-(DFT)[17] (see also Hesselmann and Jansen[18]). SAPT yields detailed information on the interactions by decomposing the potential into physically interpretable components and also enables connection with the asymptotic regime and with the properties of the interacting monomers (see, for example, Podeszwa et al.[19] for a recent application of SAPT(DFT)). However, the SAPT approach includes a reliance on the many-body expansion and, perhaps more significantly, does not allow the modeling of the breaking or formation of chemical bonds, that is, true chemistry.

Within the computationally efficient framework of DFT, advances are being made in the development of XC functionals[3] and attempts are being made to improve the existing DFT methodology. The recent overview by Grimme and co-workers[20] organizes these attempts into three groups. Workers in the first group attempt to develop or improve DFT XC functionals (GGA or hybrid and/or meta-GGA) for modeling of weak bonds. Here we mention only a few examples, and the reader is referred to Grimme et al.[20] for a more extensive list. These include the GGA XC functionals HCTH,[21] HCTH120,[22] and B97-1[21,23] and the hybrid meta-GGA functionals of Zhao and Truhlar such as

† Part of the "Max Wolfsberg Festschrift".

* Corresponding authors. Email: chris.mundy@pnl.gov (C.J.M.); greg.schenter@pnl.gov (G.K.S.).

‡ University of Minnesota.

§ Pacific Northwest National Laboratory.

10.1021/jp808767y CCC: $40.75
Published on Web 03/05/2009

M06 and M06-2X.[24] The salient feature of the aforementioned methods is that they can, in general, be used within efficient implementations of DFT and can be directly applied to problems concerning chemistry in the condensed phase. If these methods are parametrized to accurate data, they will perform well (although some testing should be done to ensure transferability). However, their inability to recover the physics of the long-range interaction puts these methods at risk of having accidental good agreement with experiment or *ab initio* approaches. Although it is a quite different approach, the attempt by Rothlisberger and co-workers[25−27] to reproduce weak interactions with standard DFT XC functionals by additional parametrization of effective core potentials (ECPs) for atoms also falls into this category.

Workers in the second and third groups do not rely on error cancellations but rather attempt to add the missing long-range correlation or dispersion component to the DFT functional. Thus, the interaction energy from these approaches should have the correct asymptotic behavior. Those in the second group attempt to add the missing component via an orbital-based or truly nonlocal correlation functional supplement to DFT. Two examples are the vdW-DF approach of the group of Langreth and Lundqvist[28] and the similar ACFDT-DFT approach of Harl and Kresse.[29] However, these methods may be too expensive to see adoption outside the groups which developed them. While these methods hold an advantage in that they do not require parametrization, the accuracy of the potentials obtained with them may be lower than required. For example, the interaction energy of Ar_2 and Kr_2 given by the vdW-DF approach[28] differs substantially from accurate calculations; the potential wells for Ar_2 and Kr_2 are too deep by 60% and 40%, respectively, and both are shifted outward by 5%.[30] The error in the well depths is comparable to those of DFT-GGA potentials such as PBE, except that PBE generally makes the well depths too shallow rather than too deep. However, the ACFDT-DFT(PBE) approach[29] for Ar fcc solid does produce good results.

The third group of approaches may be labeled collectively by the term DFT-D. They are based on the HF-D method (see Douketis et al.,[31] Wu et al.,[5] and additional references therein), which is relatively successful for rare gases and other simple systems. In these methods the Hartree−Fock or DFT interaction energy is supplemented by a (damped) long-range dispersion contribution calculated from (possibly predetermined) long-range dispersion coefficients. DFT-D methods thus require use of DFT XC functionals which behave similarly[5,32] to HF and have a minimum of attraction (e.g., revised versions of PBE[33] such as revPBE[34] or RPBE[35] or, alternatively, BLYP,[36,37] B3LYP,[38] etc.), thus avoiding the possible double-counting of the long-range correlation, as occurs with, e.g., PW91.[39] DFT-D methods have been used by Scoles,[5,32] Elstner[40,41] (who, however, supplemented an approximate DFT interaction energy), Wu and Yang,[42] Grimme,[20,43] Parrinello,[44] and Ortmann.[45] The various implementations of DFT-D differ in which DFT XC functional is used, in how the dispersion coefficients are obtained, in the damping function that is used, and in whether terms past the leading term $-C_6 f(r) r^{-6}$ are included (here, r is the intermonomer separation, $f(r)$ is a damping function, and C_6 is the leading dispersion coefficient; note that inclusion of higher-order coefficients is needed for greater accuracy[5,32]). The reader is referred to Zimmerli et al.[44] for a comparative study of various DFT-D schemes for approximating the interaction energy of water−benzene. A possible shortcoming of many DFT-D approaches is that the dispersion coefficients are not updated during the course of the simulation and thus will not be consistent with possible changes in electronic structure due to chemical reactions. In addition, atom−atom coefficients are needed to allow for the breaking/formation of bonds and also for the description of intramolecular dispersion interactions present in, e.g., large organic molecules. A possible candidate for a self-consistent, atom-based approach is that of Silvestrelli,[46] who used DFT with maximally localized Wannier function centers to localize charge density and to compute the effective dispersion. This approach is similar to that of Becke and Johnson,[47] who demonstrated that the position-dependent dipole moment of the exchange hole can be used to generate dispersion interactions between closed-shell systems.

In this work we present a theory motivated by the need to perform accurate statistical mechanical sampling and chemistry in the condensed phase. Recently, a self-consistent polarization (SCP) approach in combination with a semiempirical electronic structure method, implemented by Chang et al.,[48] was used to obtain good results for water clusters. Despite its success, one drawback of the aforementioned approach was the requirement of extensive parametrization. By replacing the semiempirical method with DFT, which is a more *ab initio* electronic structure method, most of the parametrization is eliminated. The salient feature of SCP-DFT is that it is based on linear response theory,[49,50] allowing one to simultaneously and self-consistently correct the DFT interaction with auxiliary polarization density, thus recovering the correct classical multipole polarization and polarizabilities. The quantum mechanical treatment of this additional polarization yields the celebrated London dispersion formula. Therefore, with the addition of a single parameter (for atoms), SCP-DFT provides a self-consistent picture of polarization and dispersion and enables one to recover the interaction energy including the dispersion component, which is otherwise completely missing from the local and semilocal XC functionals.

To this end, we performed a comprehensive test of SCP-DFT for argon, a case study in weak interaction. We compare results obtained using SCP-DFT both to experiment and also to those obtained using potentials ranging from a simple Lennard-Jones potential to benchmark-quality, complex many-body potentials which had been obtained by fitting the potential parameters to spectroscopic measurements (the potential of Aziz[51]) or to accurate *ab initio* calculations on the dimer (the CCSD(T)/CBS potential of Patkowski et al.[52]) and the trimer (the SAPT three-body potential of Lotrich et al.[53] and the CCSD(T) calculations of Podeszwa et al.[54]). We find that our results for the dimer potential, second virial coefficients, cluster cohesion energies, liquid structure, and fcc solid are in excellent agreement with the benchmarks.

2. Self-Consistent Polarization Density Functional Theory

2.1. Definition of the Method. The SCP-DFT approach has been implemented within the CP2K package[55] and is described in detail below. We write the DFT energy functional as

$$E_{\mathrm{DFT}}[\rho_{\mathrm{DFT}}] = T[\rho_{\mathrm{DFT}}] + E_{\mathrm{XC}}[\rho_{\mathrm{DFT}}] + E_{\mathrm{H}}[\rho_{\mathrm{DFT}}] \quad (1)$$

where $T[\rho_{\mathrm{DFT}}]$ and $E_{\mathrm{XC}}[\rho_{\mathrm{DFT}}]$ are kinetic energy and exchange-correlation functionals, respectively, and E_{H} is the Hartree functional,

$$E_{\mathrm{H}}[\rho_{\mathrm{DFT}}] = \int \mathrm{d}\mathbf{r}\, \mathrm{d}\mathbf{r}' \frac{\rho_{\mathrm{DFT}}(\mathbf{r})\rho_{\mathrm{DFT}}(\mathbf{r}')}{|\mathbf{r} - \mathbf{r}'|} \quad (2)$$

We supplement the DFT charge density, ρ_{DFT}, with the SCP charge density, ρ_{SCP}, to construct the total charge density, $\rho = \rho_{\mathrm{DFT}} + \rho_{\mathrm{SCP}}$. Within a Kohn−Sham representation,

$$\rho_{\mathrm{DFT}}(\mathbf{r}) = \sum_A Z_A \delta(\mathbf{r} - \mathbf{r}_A) - \sum_{\gamma,\mu,\nu} P^{\gamma}_{\mu\nu}\phi_\mu(\mathbf{r})\phi_\nu(\mathbf{r}) \quad (3)$$

where $P^{\gamma}_{\mu\nu}$ is the density matrix corresponding to spin γ, $\phi_\mu(\mathbf{r})$ is an atomic basis set centered on the position $\mathbf{r}_\mu$, and Z_A are core charges located at positions $\mathbf{r}_A$. The SCP density is represented as

$$\rho_{\mathrm{SCP}}(\mathbf{r}) = \sum_\alpha c_\alpha \chi_\alpha(\mathbf{r}) \quad (4)$$

where $\chi_\alpha(r)$ are auxiliary basis functions. We supplement the DFT energy functional as

$$E[\rho_{\mathrm{DFT}}, \rho_{\mathrm{SCP}}] = T[\rho_{\mathrm{DFT}}] + E_{\mathrm{XC}}[\rho_{\mathrm{DFT}}] + E_{\mathrm{H}}[\rho_{\mathrm{DFT}}] + E^{(e)}_{\mathrm{DFT\text{-}SCP}} + E^{(N)}_{\mathrm{DFT\text{-}SCP}} + E_{\mathrm{SCP\text{-}SCP}} + E^{\mathrm{disp}}_{\mathrm{SCP}} \quad (5)$$

where the SCP charge density interacting with the DFT electron density is

$$E^{(e)}_{\mathrm{DFT\text{-}SCP}} = -\sum_{\mu,\nu,\alpha} P^T_{\mu\nu} c_\alpha (\mu\nu|\alpha) f_{\mu\nu\alpha} \quad (6)$$

with Coulomb integrals

$$(\mu\nu|\alpha) = \int \mathrm{d}\mathbf{r}\, \mathrm{d}\mathbf{r}' \frac{\phi_\mu(\mathbf{r})\phi_\nu(\mathbf{r})\chi_\alpha(\mathbf{r}')}{|\mathbf{r} - \mathbf{r}'|} \quad (7)$$

The SCP charge density interacting with the DFT core density is given by

$$E^{(N)}_{\mathrm{DFT\text{-}SCP}} = \sum_{A,\alpha} Z_A c_\alpha (A|\alpha) f_{A\alpha} \quad (8)$$

with Coulomb integrals

$$(A|\alpha) = \int \mathrm{d}\mathbf{r}' \frac{\chi_\alpha(\mathbf{r}')}{|\mathbf{r}_A - \mathbf{r}'|} \quad (9)$$

Here $f_{\mu\nu\alpha}$ and $f_{A\alpha}$ are screening functions that damp the Coulomb interactions when they involve auxiliary sites at short distances: $f_{A\alpha} = 0$ when $\mathbf{r}_A = \mathbf{r}_\alpha$ and $f_{\mu\nu\alpha} = 0$ when $\mathbf{r}_\mu = \mathbf{r}_\nu$, $\mathbf{r}_\mu = \mathbf{r}_\alpha$, or $\mathbf{r}_\nu = \mathbf{r}_\alpha$. The SCP-SCP self-interaction is given by

$$E_{\mathrm{SCP\text{-}SCP}} = \frac{1}{2}\sum_{\alpha,\beta} c_\alpha c_\beta \left\{ \frac{1}{a_\alpha}\delta_{\alpha,\beta} + (\alpha|\beta) f_{\alpha\beta} \right\} \quad (10)$$

where the Coulomb integral is given by

$$(\alpha|\beta) = \int \mathrm{d}\mathbf{r}\, \mathrm{d}\mathbf{r}' \frac{\chi_\alpha(\mathbf{r})\chi_\beta(\mathbf{r}')}{|\mathbf{r} - \mathbf{r}'|} \quad (11)$$

and $f_{\alpha\beta}$ is a screening function. The generalized polarizability is a_α. A self-consistent expression for the dispersion interaction is

$$E^{\mathrm{disp}}_{\mathrm{SCP}} = -\frac{1}{8}\sum_{\alpha,\beta} \frac{I_\alpha I_\beta}{I_\alpha + I_\beta} a_\alpha a_\beta (\alpha|\beta)^2 f^2_{\alpha\beta} \quad (12)$$

The self-consistent procedure consists of the two variational conditions,

$$\frac{\delta}{\delta\rho_{\mathrm{DFT}}} E[\rho_{\mathrm{DFT}}, \rho_{\mathrm{SCP}}] = 0 \quad (13)$$

and

$$\frac{\delta}{\delta\rho_{\mathrm{SCP}}} E[\rho_{\mathrm{DFT}}, \rho_{\mathrm{SCP}}] = 0 \quad (14)$$

The DFT charge density is subject to the orthonormality constraint. Explicitly, if the density matrix is represented in terms of the molecular orbitals, $C^{\gamma}_{\mu i}$,

$$P^{\gamma}_{\mu\nu} = \sum_i n^{\gamma}_i C^{\gamma}_{\mu i} C^{\gamma}_{\nu i} \quad (15)$$

where n^{γ}_i are orbital occupancies, to give

$$\sum_{\mu,\nu} C^{\gamma}_{\mu i} S_{\mu\nu} C^{\gamma}_{\nu j} = \delta_{ij} \quad (16)$$

with

$$S_{\mu\nu} = \int \mathrm{d}\mathbf{r}\, \phi_\mu(\mathbf{r})\phi_\nu(\mathbf{r}) \quad (17)$$

The only constraint on the SCP charge density is that no extra charge is generated (net monomer SCP moment is zero),

$$\int d\mathbf{r}\rho_{\mathrm{SCP}}(\mathbf{r}) = 0 \quad (18)$$

The variational procedure leads to the standard self-consistent field equations

$$F^{\gamma}_{\mu\nu} C^{\gamma}_{\nu i} = S_{\mu\nu} C^{\gamma}_{\nu i} \varepsilon_i \quad (19)$$

where the Fock matrix (Kohn−Sham matrix)

$$F^{\gamma}_{\mu\nu} = \frac{\partial}{\partial P^{\gamma}_{\mu\nu}} E[\rho_{\mathrm{DFT}}, \rho_{\mathrm{SCP}}] \quad (20)$$

is decomposed into the unmodified DFT Fock matrix, $F^{\gamma(0)}_{\mu\nu}$, and the perturbation due to SCP, $\Delta F^{\gamma}_{\mu\nu}$,

$$F^{\gamma}_{\mu\nu} = F^{\gamma(0)}_{\mu\nu} + \Delta F^{\gamma}_{\mu\nu} \quad (21)$$

where

$$\Delta F^{\gamma}_{\mu\nu} = -\sum_\alpha c_\alpha (\mu\nu|\alpha) f_{\mu\nu\alpha} \quad (22)$$

In terms of SCP coefficients, c_α, the SCP variational expression becomes

$$\frac{\partial}{\partial c_\alpha} E[\rho_{\mathrm{DFT}}, \rho_{\mathrm{SCP}}] = 0 \quad (23)$$

or

$$\sum_\beta c_\beta \left\{ \frac{1}{a_\alpha}\delta_{\alpha,\beta} + (\alpha|\beta) f_{\alpha\beta} \right\} - \sum_{\mu,\nu} P^T_{\mu\nu} (\mu\nu|\alpha) f_{\mu\nu\alpha} + \sum_A Z_A (A|\alpha) f_{A\alpha} = 0 \quad (24)$$

leading to the linear response of the SCP coefficients to the external multipole Coulomb field

$$c_\alpha = a_\alpha \Phi_\alpha \quad (25)$$

where the multipole field is given by

$$\Phi_\alpha = -\sum_\beta c_\beta (\alpha|\beta) f_{\alpha\beta} + \sum_{\mu,\nu} P^T_{\mu\nu} (\mu\nu|\alpha) f_{\mu\nu\alpha} - \sum_A Z_A (A|\alpha) f_{A\alpha} \quad (26)$$

2.2. Screening Function. We write for the pair screening function

$$f_{\mu\nu} = 1 - e^{-(\sigma^\mu+\sigma^\nu)R_{\mu\nu}}\left(1 + \frac{1}{2}(\sigma^\mu + \sigma^\nu)R_{\mu\nu}\right) \quad (27)$$

where $R_{\mu\nu} = |\mathbf{r}_\mu - \mathbf{r}_\nu|$ and the coefficients σ^μ determine the effective screening length. We will construct triplet screening functions as

$$f_{\mu\nu\alpha} = 1 - (1 - f_{\mu\nu})(1 - f_{\mu\alpha})(1 - f_{\nu\alpha}) \quad (28)$$

In initial implementations, we will take the limit $\sigma^\mu \to \infty$, giving

$$f_{\mu\nu} = 1 - \delta_{A_\mu A_\nu} \quad (29)$$

where A_μ is an atom site label associated with orbital μ. In future work we will consider other forms for this screening and its relation to the parametrization and efficiency of the method.

2.3. Dispersion. To evaluate the expression for the dispersive interaction between two auxiliary charge densities, first consider the energy for an auxiliary charge density in an external multipole field,

$$E = \sum_\alpha \left(\frac{c_\alpha^2}{2a_\alpha} - c_\alpha\phi_\alpha\right) \quad (30)$$

With $\partial E/\partial c_\alpha = 0$,

$$c_\alpha = a_\alpha\phi_\alpha \quad (31)$$

This represents the response of the auxiliary polarization density matrix, c_α, to an external field, ϕ_a, where a_α is a generalized polarizability. For interacting auxiliary charge densities, the energy is

$$E = \frac{1}{2}\sum_{\alpha,\beta} c_\alpha c_\beta\left\{\frac{1}{a_\alpha}\delta_{\alpha,\beta} + (\alpha|\beta)f_{\alpha\beta}\right\} \quad (32)$$

If we consider the interaction as a quantum mechanical perturbation converting density coefficients c_α to quantum mechanical operators $\hat{c}_\alpha$,

$$\hat{V} = \sum_{\alpha<\beta} \hat{c}_\alpha\hat{c}_\beta(\alpha|\beta)f_{\alpha\beta} \quad (33)$$

then a second-order perturbation theory expression for the dispersion energy may be written as

$$E^{\text{disp}} = \sum_{\alpha<\beta}\sum_{\bar{\alpha}<\bar{\beta}}(\alpha|\beta)f_{\alpha\beta}(\bar{\alpha}|\bar{\beta})f_{\bar{\alpha}\bar{\beta}} \times \sum_{k\neq 0}\sum_{l\neq 0}\frac{\langle 0|\hat{c}_\alpha|k\rangle\langle 0|\hat{c}_\beta|l\rangle\langle k|\hat{c}_{\bar{\alpha}}|0\rangle\langle l|\hat{c}_{\bar{\beta}}|0\rangle}{E_0^\alpha + E_0^\beta - E_k^\alpha - E_l^\beta} \quad (34)$$

where E_k^α denotes an excitation of the uncoupled Hamiltonian with potential energy $c_\alpha^2/2a_\alpha$ on site α, and α and $\bar{\alpha}$ denote different multipoles on an identical site. In terms of this notation, the multipole dispersion interaction may be written in a "Casimir−Polder" form (the reader is referred to, e.g., the work of Longuet−Higgins[56] and also of Misquitta et al.[17] and additional references therein) as

$$E^{\text{disp}} = -\frac{1}{2\pi}\int_0^\infty d\omega \sum_{\alpha<\beta}\sum_{\bar{\alpha}<\bar{\beta}} a_{\alpha,\bar{\alpha}}(i\omega)a_{\beta,\bar{\beta}}(i\omega)(\alpha|\beta)f_{\alpha\beta}(\bar{\alpha}|\bar{\beta})f_{\bar{\alpha}\bar{\beta}} \quad (35)$$

where $a_{\alpha,\bar{\alpha}}(i\omega)$ is a generalized, multipole dynamic polarizability,

$$a_{\alpha,\bar{\alpha}}(\omega) = 2\sum_{k\neq 0}\frac{E_k^\alpha - E_0^\alpha}{(E_k^\alpha - E_0^\alpha)^2 - \omega^2}\langle 0|\hat{c}_\alpha|k\rangle\langle k|\hat{c}_{\bar{\alpha}}|0\rangle \quad (36)$$

If it is assumed that

$$a_{\alpha,\bar{\alpha}}(i\omega) = a_\alpha\frac{I_\alpha^2}{I_\alpha^2 + \omega^2}\delta_{\alpha,\bar{\alpha}} \quad (37)$$

then we recover the generalized, multipole, London dispersion expression that is consistent with the multipole polarizabilities used in eq 12.

3. Computational Details

The DFT and SCP-DFT calculations were performed using the CP2K/Quickstep package[55,57] in conjunction with the BLYP[36,37] XC functional and Goedecker−Teter−Hutter-style pseudopotential.[58−60] Our Ar_2 interaction energy calculations using BLYP revealed that the DZVP basis set gave similar results to the nearly complete and essentially BSSE-free QZV3P basis set (see Figure 1). The former basis was then used in the majority of the calculations, while the latter basis continued to serve as a benchmark.

In CP2K, nonperiodic calculations (i.e., cluster calculations) are performed using the nonperiodic option with the Martyna−Tuckerman[61] Poisson solver. Alternatively, for uncharged and nonpolar systems, it is simple to use periodic boundary conditions (PBC) with a large amount of vacuum to reduce the spurious interactions between images. We found the latter option with a cubic box of side length of 30 Å performed well in terms of lower memory and time requirements. In order to reduce grid effects for our dimer and trimer energy calculations, the energy cutoff used for expansion of the electron density in plane waves was set to a relatively high value of 500 Ry while the SCF energy convergence threshold was tightened to 10^{-8} hartree/atom. The wave function optimization was performed with the orbital transformation (OT) method using the conjugate gradient (CG) algorithm. For our cluster calculations, the plane wave cutoff was 200 Ry, energy convergence was 10^{-6} hartree/atom, and convergence of gradient was 4.5×10^{-4} hartree/Å.

The liquid argon calculations were performed in a supercell containing 96 atoms. The cell parameter of the cubic box containing the sample was chosen to be 16.7 Å, resulting in a density of 1.37 g/mL, which is in reasonable agreement with the density of 1.396 g/mL reported by the *CRC Handbook*[62] for liquid argon at its boiling point (87.3 K). The initial configuration was obtained using standard Monte Carlo (MC) in the *NpT* ensemble with a Lennard-Jones (LJ) argon potential. The LJ parameters for argon, $\sigma = 3.40$ Å and $\varepsilon = 114.99$ K, were determined from the precise vapor−liquid equilibrium (VLE) simulations for Lennard-Jonesium by Potoff and Panagiopoulos[63] and the experimental argon VLE data of Michels et al.[64] by taking the appropriate ratios of the critical properties of Lennard-Jonesium to the experimental critical properties of argon, i.e., $\varepsilon = T_c/T_c^*$ and $\sigma = (\rho_c^*/\rho_c)^{1/3}$. It is important to note here that this parametrization leads to an effective LJ potential that is appropriate for condensed phases and implicity includes many-body terms and nuclear quantum effects.[65] A well-equilibrated configuration of LJ argon was used as the starting configuration for a SCP-DFT molecular dynamics (MD) simulation in a periodically replicated cubic cell. The MD simulation was performed in the *NVT* ensemble using the method of Nosé and Hoover[66−69] with a time step of 0.5 fs. The system was equilibrated for 10 ps, followed by 25 ps of production for the accumulation of averages. The last 10 ps are presented in our final results. The distance cutoff for the summation of the dispersion contribution to the SCP-DFT energy was 11 Å. The cutoff for the electron density was 200 Ry, while the SCF energy convergence threshold was 10^{-6} hartree/atom. The OT method[70]

with the DIIS minimizer was used in the dynamics calculations for the optimization of the wave function.

The SCP-DFT calculations on the Ar face-centered cubic (fcc) solid were performed at the Γ-point only (due to limitations of CP2K) using a 32 atom cell. The nearest-neighbor separation, r_{ss} (or equivalently, the lattice parameter $a = \sqrt{2}r_{ss}$), was changed, and the cell lattice vectors and atomic positions were likewise scaled as DFT calculations were performed, thus obtaining the cohesion energy per atom as a function of r_{ss}. The cohesion energy per atom is given by $E_{coh}(r_{ss}) = (E_n(r_{ss}) - nE_1)/n$, where E_n and E_1 are the energies of n atoms and 1 atom, respectively. Due to numerical artifacts associated with a finite charge density grid, and to ensure a smooth cohesion energy curve, it was necessary to compute the reference energy of the argon monomer in the identical cell, that is, to use the value $E_1(r_{ss})$ in the above equation. The distance cutoff for the summation of the dispersion contribution to the SCP-DFT energy was 11 Å. To ensure accuracy, a density cutoff of 300 Ry was utilized with an SCF energy convergence threshold of 10^{-8} hartree/atom. Identical results were obtained when a higher density cutoff of 1000 Ry was used. To check convergence with respect to cell size (or, equivalently, k-points), we confirmed that use of a 108 atom cell also yielded nearly identical results.

4. Parameterization

As alluded to in section 1, our choice in developing the SCP-DFT theory is that many of the parameters are determined for us by the choice of XC functional. Thus, in principle, for structureless particles such as argon, the parametrization of the potential should be straightforward. Indeed this is the case. The parameters that must be determined for SCP-DFT are the choice of the auxiliary basis set and the parameters for the polarizability, a_α, and London dispersion, I_α. In CP2K/QUICKSTEP the basis set is the standard contracted Gaussian basis set. The auxiliary basis set is of the same form, namely, $\chi_\alpha(\mathbf{r}) = \sum_i d_{i\alpha} g_i(\mathbf{r})$ and yields the (unnormalized) auxiliary density via eq 4. Here, α is the index for the density, d is the contraction coefficient, and g is a primitive Gaussian function with width determined by a single parameter ζ (in units of 1/bohr^2). In preliminary applications we have used only a single Gaussian function, of p symmetry. The latter choice ensures that the asymptotic behavior of the argon dimer interaction energy, dominated by the dispersion contribution defined by eq 12, will be of the correct r^{-6} form.

The finite-field approach was used within CP2K to fit the SCP parameter a_α in order to reproduce the accurate static dipole polarizability $\alpha = 11.085 \pm 0.06$ au recently recommended by Lupinetti and Thakkar[71] based on their finite field, large basis set CCSD(T) calculations (with an estimate of the relativistic correction), a theoretical value very close to the experimental one of 11.075 ± 0.006 au.[62]

The change in energy of a neutral atom in the presence of an applied electric field of strength $F = |\boldsymbol{F}|$ is given by

$$\Delta E = E(F) - E(0) = \frac{-\alpha F^2}{2!} - \frac{\gamma F^4}{4!} - \cdots \quad (38)$$

where $E(F)$ and $E(0)$ are the field-dependent and field-free energies, α is the polarizability, and γ is the hyperpolarizability. Ignoring the hyperpolarizability, we have

$$\Delta E = \frac{-\alpha F^2}{2} \quad (39)$$

We generated fields by placing point charges $\pm Q$ (where Q ranged from 0.1 to 5.0 au) at positions $z = \pm 5$ Å relative to an argon atom at the origin (thus ensuring that the field gradient vanished at the origin). Hence the field at the origin,

$$\boldsymbol{F}(\mathbf{0}) = -\frac{2Q}{Z^2}\hat{\boldsymbol{z}} \quad (40)$$

ranged from approximately 0.00224 to 0.112 au. For comparison, Lupinetti and Thakkar[71] used fields ranging from 0.0044 to 0.0176 au.

Since $E(0)$, $E(F)$, and ΔE are all parametrically dependent on the SCP parameters ζ and a_α, we performed calculations for various fixed values of ζ and a_α, each time varying the fields so as to extract α from a least-squares fit of ΔE versus F in eq 39. As ζ increases the argon atom becomes more point-charge-like. Finally we chose a reasonable $\zeta = 0.2$ and only considered p (or dipole) polarization density functions. This choice of ζ reflects our choice of screening function in that in the present study we rely on the natural screening due to the overlap of two overlapping Gaussian charges. For argon this choice of trivial screening allows for a stable theory. However, a more robust choice for the screening will be investigated in future publications. Thus, utilizing only the dipole auxiliary charge density, we fix $a_\alpha = 2.91 \times 10^{-4}$ yielding a polarizability, $\alpha = 11.086 \pm 0.001$ au, which is in very good agreement with the target value of 11.085 au.[71]

After fixing ζ and a_α to reproduce the known polarizability, one additional parameter I_α is needed to reproduce the argon dimer potential of Aziz,[51] which is generally accepted as the most accurate empirical potential. Specifically, we chose $I_\alpha = 3.977$ au to reproduce the interaction energy of the Aziz potential at an interatomic separation of 3.60 Å. The resulting SCP-DFT value of −0.2581 kcal/mol agrees quite nicely with the Aziz value of −0.2579 kcal/mol.

One should be reminded that unlike calculations with LDA or PBE XC functionals,[32] the BLYP argon dimer potential is completely repulsive. This feature actually facilitates the use of the SCP-DFT correction to account for the missing attractive component of the interaction energy.

5. Results

5.1. Dimer Potential. We computed the Ar_2 potential over the range $r = 2.10-10.0$ Å at every 0.1 Å. Our SCP-DFT potential agrees quite nicely with the Aziz potential,[51] our benchmark empirical potential, in the region of the repulsive wall and the potential well (see top panel of Figure 1). We also compared our results to the highly accurate *ab initio* CCSD(T) with complete basis set limit extrapolation potential of Patkowski et al,[52] (CCSD(T)/CBS), and the effective Lennard-Jones (LJ) potential for argon described above (which is, of course, too repulsive at short separation). The largest discrepancy of the SCP-DFT potential from the benchmarks is in the region of the tail, where it is too negative (see bottom panel of Figure 1). Since the tail region is given by the dispersion expression in eq 12, and our use of p functions ensures an r^{-6} falloff, to extract additional information about this region (and also to enable efficient calculation of the virial coefficients, see below), we fitted the calculated SCP-DFT interaction energies in the range $r = 6.5-7.0$ Å using the form $-C_6 r^{-6}$, and obtained $C_6 = 130$ au, which is too large compared to the correct value[72] of 64.691 au. This discrepancy is likely due to our attempt to model the dispersion interaction present in the Aziz potential (which contains also C_8 and C_{10} coefficients) using only the leading-order term. In future, we will use d auxiliary functions in addition to the p functions, together with appropriate screening

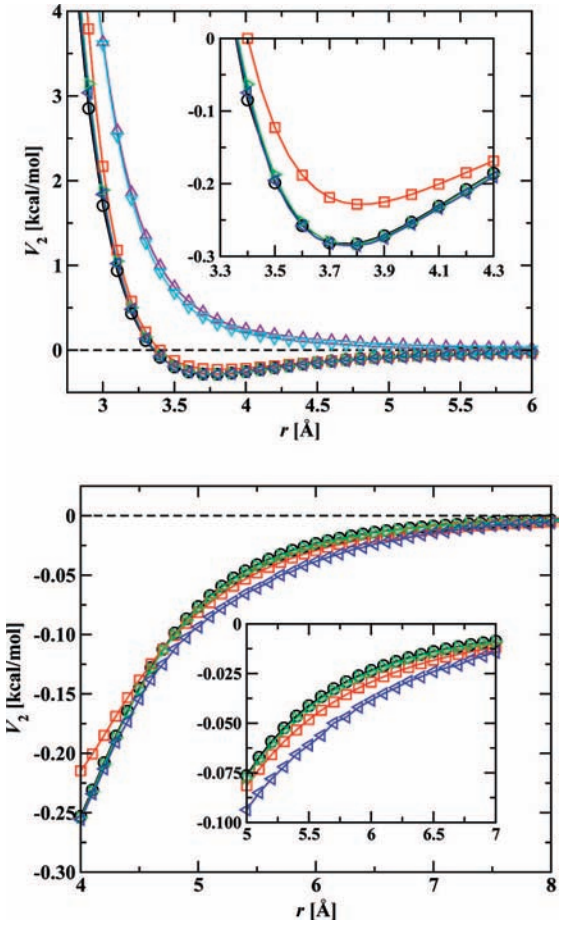

Figure 1. Interatomic potentials for Ar_2. The top and bottom panels show the whole potential and its tail, respectively. The insets show close-ups. Aziz[51] (black circles), CCSD(T)/CBS[52] (green right triangles), LJ (red squares), BLYP/QZV3P (purple up triangles), BLYP/DZVP (cyan down triangles), and SCP-DFT (blue left triangles). Lines are shown to guide the eye.

or damping functions, and this is expected to lead to better performance in the tail region.

Table 1 compares the minimum separations r_e and the binding energies D_e of Ar_2 obtained from different methods to *ab initio* and empirical benchmarks. Upon examining the pure DFT results, we see that the LDA and PW91 XC functionals overbind the dimer, whereas PBE and revPBE underbind and BLYP is purely repulsive. Of the corrected DFT methods, the DCACP-DFT method[26] gives a result that is in good agreement with the MP2 value to which it was fit (basis-set converged MP2, however, overbinds Ar_2). However, we stress that this approach is not physical and cannot reproduce the asymptotic limit of the interaction energy curve. As pointed out by Scoles and coworkers,[5,32] among others, the DFT-D approaches, although justified on physical grounds, require the use of an XC functional that has minimal attraction in order to avoid double-counting. By adding a dispersion correction to PW91, which already overbinds, Ortmann et al.[45] err in this regard. The more complex vdW-DFT[28] model also overbinds. The method of Becke and Johnson[47] underbinds the dimer, while that of Silvestrelli[46] yields a minimum separation that is too large by over 0.2 Å. Our SCP-DFT result, which requires fitting of only two independent parameters, obviously agrees quite well with the benchmarks. As the LJ potential parameters were determined from VLE properties, it is not surprising that it does not perform as well as the other methods for the dimer.

TABLE 1: Argon Dimer Minimum Atom−Atom Separation r_e and Binding Energy D_e, As Obtained from the Literature or by Harmonic Fits to Our Results in the Region of the Minimum[a]

method or potential	r_e (Å)	D_e (kcal/mol)
DFT		
LDA[32]	3.42	0.698
PW91[45]	3.97	0.318
PBE[32]	4.04	0.137
revPBE[46]	4.67	0.039
BLYP/QZV3P	n/a	n/a
BLYP/DZVP	n/a	n/a
DFT with corrections		
DCACP-DFT(BLYP)[b] [26]	3.9	0.23
vdW-DF(revPBE)[c] [28]	3.9	0.46
DFT-D(PW91) (Ortmann)[45]	3.97	0.353
DFT-D(B97−1) (Becke)[47]	3.9	0.240
DFT-D(revPBE) (Silvestrelli)[46]	4.03	0.274
SCP-DFT	**3.788**	**0.2857**
ab initio calculations and benchmarks		
MP2[d] [85]	3.88	0.2253
MP2[32]	3.77	0.311
CCSD(T)/CBS[52]	3.767	0.2838
empirical calculations and experimental benchmarks		
LJ (effective 2 body)[e]	**3.82**	**0.229**
Aziz[51]	3.757	0.2846
experiment[86]	3.761	0.284

[a] Note that zero-point effects are not included. "n/a" indicates that the curve is repulsive. Results of this work are highlighted in bold font. [b] von Lilienfeld et al.[25] fit the parameters of their optimized effective core potential to reproduce their MP2/aug-cc-pVTZ results. [c] From Table 4 of Bruch et al.[87] [d] A relatively small basis set was used in this work. [e] $r_e = 2^{1/6}\sigma$ and $D_e = -V_{LJ}(r_e)$, but this effective potential implicitly accounts for zero-point effects.

5.2. Second Virial Coefficients. The second virial coefficient, $B_2(T)$, of a pure substance or mixture depends solely on the two-body intermonomer potential.[73] Due to the importance of the virial equation of state in thermal physics, experimental data exists for many substances. This allows one to readily assess the accuracy of model potentials. The second virial coefficients can be expressed as the sum of the classical term and quantum corrections,

$$B_2(T) = B_c(T) + B_q(T) \tag{41}$$

For an atom−atom two-body potential $V_2(r)$,

$$B_c(T) = -2\pi \int_0^\infty dr\, r^2 [e^{-V_2(r)/k_B T} - 1] \tag{42}$$

where T is the temperature and k_B is Boltzmann's constant. Quantum corrections become important at lower temperatures and can be expressed as a series in h^2, where h is Planck's constant.[73] At the lowest temperature that we considered, 100 K, the first term in this expansion is sufficient to account for more than 95% of the full quantum correction[74] to the virial coefficient of Ar (about 1.50 $cm^3\ mol^{-1}$ with various potentials[52]). Thus, one can approximate the quantum corrections by their leading term, given by

$$B_q(T) = \frac{h^2}{24\pi m (k_B T)^3} \int_0^\infty dr\, r^2\, e^{-\beta V_2(r)} \left(\frac{dV_2}{dr}\right)^2 \tag{43}$$

For the LJ model potential, converged results were obtained using trapezoidal numerical integration over the range 0−50 Å with a step size of 0.001 Å. For the SCP-DFT potential, these

TABLE 2: Comparison of Second Virial Coefficients (in cm^3/mol) at Various Temperatures (in K)

T	expt[75]	CCSD(T)/CBS[52]	Aziz[51,52]	LJ	SCP-DFT
100.0	−183.5 ± 1.0	−181.84	−181.98	−159.30	−227.73
150.0	−86.2 ± 1.0	−85.81	−85.99	−77.63	−114.12
200.0	−47.4 ± 1.0	−47.63	−47.89	−43.29	−68.13
250.0	−27.9 ± 1.0	−27.37	−27.70	−24.57	−43.47
300.0	−15.5 ± 0.5	−14.92	−15.30	−12.88	−28.18
400.0	−1.0 ± 0.5	−0.60	−1.03	0.78	−10.41
500.0	7.0 ± 0.5	7.26	6.78	8.37	−0.55
600.0	12.0 ± 0.5	12.13	11.62	13.12	5.63
700.0	15.0 ± 1.0	15.37	14.85	16.32	9.81
800.0	17.7 ± 1.0	17.66	17.12	18.58	12.77
900.0	20.0 ± 1.0	19.32	18.77	20.24	14.96
1000.0	22.0 ± 1.0	20.56	20.00	21.50	16.63

integration parameters remained the same, but for numerical and efficiency reasons, the integration was performed piecewise over three regions. In the region $r = 0-2.1$ Å, excellent results were obtained simply by setting the potential to a large positive value (resulting in a Mayer function equal to −1). For $r = 2.1-7.0$ Å, local cubic splines were used to interpolate the potential. Finally, in the region $r = 7.0-50$ Å, the potential was extrapolated using the form fitted in section 5.1, $-C_6r^{-6}$.

The virial coefficients are presented in Table 2 and Figure 2. Compared to the experimental data compiled by Dymond and Smith,[75] and the highly accurate results of the Aziz[51] and CCSD(T)/CBS[52] potentials, which are in excellent agreement over the entire temperature range, the virial coefficients obtained using the SCP-DFT potential are too negative while the LJ virial coefficients have the opposite problem. These deviations are largest at low temperatures, where the magnitude of the virial coefficient is most dependent on the volume of the potential well. These results could have been predicted from the fact that the overly negative tail for the SCP-DFT potential leads to a volume of the potential well that is too large while the effective LJ potential has a minimum that is too shallow (see Figure 1). Thus the SCP-DFT potential performs nearly as well as the effective LJ potential in terms of percent deviation from experiment. This in itself is an accomplishment given that the bare DFT produces a repulsive two-body potential.

5.3. Cluster Cohesion Energies. As a further test of the transferability of the SCP-DFT potential, we calculated the energies of small argon clusters containing $n = 2-10$ atoms. The configurations were optimized for the Aziz potential[51] by Naumkin et al.[76] and are downloadable from the Cambridge Cluster Database.[77] Our cluster calculations were performed using the LJ, BLYP/DZVP, BLYP/QZV3P, and SCP-DFT potentials. Note that the Aziz potential used by Naumkin and co-workers is strictly a two-body potential, while the LJ potential is an effective two-body potential (i.e., fit to bulk properties), and the BLYP potentials include many-body nonadditive effects. Use of a pure two-body potential in the work of Naumkin et al. was justified since the many-body effects in rare gases are known to be small (though significant in the solid, see below). As Figure 3 shows, BLYP without SCP does not form mutually binding clusters. However, the decent agreement between the BLYP/DZVP and BLYP/QZV3P results shows the fast convergence of DFT methods with respect to basis set size. This justifies the choice of the DZVP basis set for the SCP-DFT calculations on the clusters. Moreover, the LJ potential results in clusters which are somewhat underbound, which is not surprising given that the dimer potential is too repulsive, while the SCP-DFT potential yields clusters which are slightly overbound. The overbinding with SCP-DFT is almost certainly due to an overestimation and wrong sign (and thus attraction rather than repulsion) of the many-body effects with BLYP; further discussion of the problems of BLYP with many-body effects appears below.

5.4. Liquid Structure. We also examined whether our excellent agreement with gas phase clusters also holds for the liquid phase by computing the radial distribution function (RDF) at 85 K. Figure 4 shows excellent agreement between the RDF obtained using SCP-DFT with the experimental RDF and the one obtained using the effective LJ potential. Note that whereas

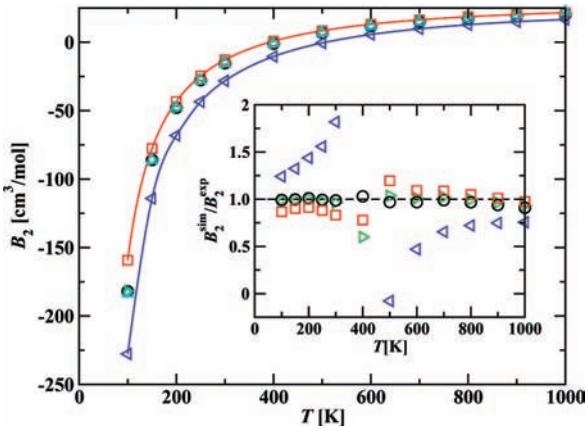

Figure 2. Second virial coefficients of argon: experiment[75] (cyan up triangles), Aziz[51,52] (black circles), CCSD(T)/CBS[52] (green right triangles), LJ (red squares), and SCP-DFT (blue left triangles). Virial coefficients for the Aziz[51] and CCSD(T)/CBS[52] potentials were calculated by Patkowski et al.[52] and are taken from Table 5 of that reference. Inset shows a plot of B_2^{sim}/B_2^{exp}. The largest deviations occur near the Boyle temperature.

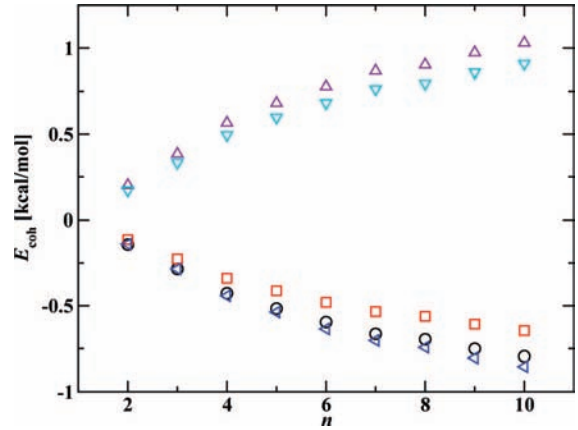

Figure 3. Cohesion energies (per atom) of Ar_n clusters for various cluster sizes n: Aziz[51] (black circles), LJ (red squares), BLYP/QZV3P (purple up triangles), BLYP/DZVP (cyan down triangles), and SCP-DFT (blue left triangles).

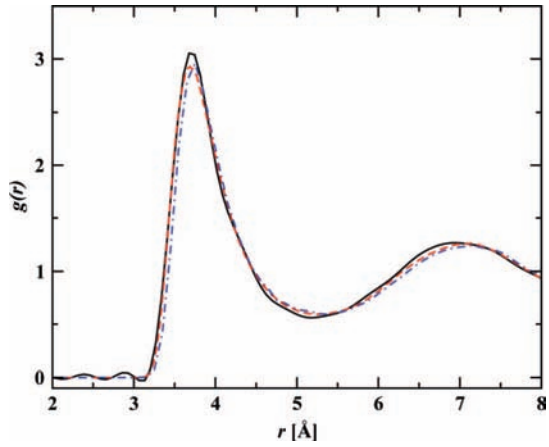

Figure 4. Radial distribution functions of liquid argon at 85 K: experiment[93] (black solid line), LJ (red dashed line), and SCP-DFT (blue dash-dotted line).

the thermodynamics and energetics of liquid argon are quite sensitive[78] to the many-body effects (see more on the role of the three-body nonadditivity in the solid below), the structure of the liquid—and therefore the RDF—is not,[78] which explains the good agreement of the SCP-DFT RDF with experiment.

5.5. FCC Solid and Role of Three-Body Nonadditivity. As the final—and more sensitive—test, we used SCP-DFT to obtain the cohesion energy of the fcc argon solid. As with the liquid and the clusters, SCP-DFT calculations were initially performed with BLYP for the DZVP basis set. However, as these results were unsatisfactory (see Figure 5 and Table 3), we decided to perform the same calculations using the more complete QZV3P basis set. Since polarization is zero in the crystal (by symmetry), the dispersion is only determined by the postprocessed London dispersion expression and does not enter the total energy through the SCF calculation. Hence calculations for SCP-DFT with BLYP/QZV3P can be performed without reparameterization. Calculations for BLYP with the QZV3P basis set showed that the BSSE in the crystal is larger than in the clusters, as a comparison of Figures 3 and 5 shows. Replacement of the BLYP/DZVP with the nearly basis-set complete BLYP/QZV3P energies in determination of the SCP-DFT cohesion energies reduces our initial error in the cohesion energy with respect to the Lotrich[79] (2 + 3 body)[51,53] benchmark from a discrepancy of −0.70 kcal/mol (−35% error) for SCP-DFT/DZVP to −0.35 kcal/mol (−17% error) for SCP-DFT/QZV3P (see Table 3).

Given that the initial success of SCP-DFT for the argon clusters and the liquid was better than the above-mentioned 0.35 kcal/mol discrepancy that we obtained for the solid, additional investigation into the reasons for this discrepancy was necessary in order to understand the limitations of SCP-DFT. To this end, it is important to remember that crystal energetics are more sensitive to many-body effects. Although the many-body effects in rare-gas clusters are small, they are known to contribute 3−7% to the cohesion energy of rare-gas solids (Ne through Xe); specifically, in Ar the many-body contribution is about 6%.[80] For this reason, we examined the leading-order many-body effect, the three-body nonadditivity, defined as

$$V_3 = E(\mathbf{r}_i, \mathbf{r}_j, \mathbf{r}_k) - E(\mathbf{r}_i, \mathbf{r}_j) - E(\mathbf{r}_i, \mathbf{r}_k) - E(\mathbf{r}_i, \mathbf{r}_k) + E(\mathbf{r}_i) + E(\mathbf{r}_j) + E(\mathbf{r}_k) \quad (44)$$

for a trimer, where the energies on the right-hand side of the equation are the total energies of the trimer, the dimers, and the monomers comprising the trimer. Asymptotically, the well-known Axilrod−Teller−Muto[81,82] triple−dipole dispersion component of the three-body nonadditivity is known to properly represent the three-body nonadditivity of rare-gas trimers, where the standard ATM term for a trimer is given by

$$V_3^{\mathrm{ATM}} = \upsilon \frac{(1 + 3\cos\theta_i \cos\theta_j \cos\theta_k)}{(r_{ij} r_{jk} r_{ik})^3} \quad (45)$$

and the triangle's side lengths and angles have their obvious meanings. We used an accurate value of the ATM parameter $\upsilon = 521.7$ au.[83]

As in Podeszwa et al.[54] we computed the leading-order nonadditive contributions to the interaction energy of argon trimers arranged in an equilateral configuration. These configurations are known to have the largest contributions to the nonadditive part of the cohesion energy of the fcc solid, although the contribution is still quite small. Figure 6 shows that BLYP (with and without SCP) gives a negative value for the three-body nonadditivity of the Ar_3 interaction energy in the region of greatest interest for the solid (3.5−4.0 Å), although the trend is correct. The correct result, given by the CCSD(T) curve, and asymptotically by the ATM curve, is positive. This figure also explains why our cluster cohesion energies are more negative than those given by the LJ potential (see Figure 3).

This behavior of BLYP is the opposite of the nonempirical DFT XC functionals (LDA, PBE, TPSS, etc.), where the three-body nonadditivity of rare gases is positive and larger than the true value, as Tkatchenko and von Lilienfeld[84] have shown. Adding an additional positive ATM term in that situation only makes the error worse, as has been observed.[84]

Since our SCP-DFT model in its present formulation does not account for the many-body dispersion that is missing in BLYP, we are at liberty to add a simple correction in the form of an ATM term. The ATM contribution to the fcc lattice energy was obtained by performing a three-body sum of eq 45 over a (nonperiodic) lattice. To obtain a value converged to 0.01 kcal/mol, it was necessary to sum over a lattice of $n = 1372$ atoms. We used a spherical cutoff of $r_{\mathrm{cut}} = 2a$ for all three side lengths, where a is the lattice constant, $a = \sqrt{2} r_{ss}$, and r_{ss} is the nearest-neighbor separation within the lattice. Near the experimental separation, at $r_{ss} = 3.7$ Å ($r_{\mathrm{cut}} = 10.4$ Å), the ATM contribution is 0.15 kcal/mol, in reasonable agreement with the three-body SAPT contribution of 0.1362 kcal/mol at $r_{ss} = 3.7508$ Å found in the work of Lotrich and Szalewicz.[79]

To simultaneously correct for the negative three-body contribution coming from BLYP and include the missing many-body dispersion, we determined that we needed to add twice the standard value of the ATM term. (Note that this analysis and the factor of 2 is only preliminary; in any case, a detailed study of the three-body corrections to the dispersion contribution is outside the scope of this work.) This addition had the effect of reducing the remaining discrepancy relative to the Lotrich[79] (2 + 3 body)[51,53] benchmark from −0.35 to only −0.07 kcal/mol (−3% error). Our final cohesion energy obtained in this manner is labeled SCP-DFT/QZV3P/2 × ATM and agrees quite well with accurate benchmarks. Table 3 compares our results for the minimum separation ($r_{ss,\,\mathrm{min}}$), the cohesion energy per atom (E_{coh}), and the bulk modulus (B_0) of fcc solid Ar with a wide set of results from the literature. Since the two-body potential provides the most important contribution to the interaction energy for rare gases, the various pure DFT XC functionals perform in an analogous manner as they did for Ar_2 (see Table 1). Of the corrected DFT approaches in the literature, ACFDT with the PBE functional does reasonably well. Our SCP-DFT/QZV3P/2 × ATM result compares very well with

TABLE 3: Argon fcc Crystal Minimum Nearest-Neighbor Separation $r_{ss,\,min}$ (and, Equivalently, Minimum Lattice Constant a_{min}), Cohesion Energy (per Atom) E_{coh}, and Bulk Modulus B_0, As Obtained from the Literature or by Harmonic Fits to Our Results in the Region of the Minimum[a]

method or potential	$r_{ss,\,min}$ (Å)	a_{min} (Å)	$-E_{coh}$ (kcal/mol)	B_0 (GPa)
		DFT		
LDA[29]	3.5	4.9	3.2	–
PW91[45]	4.3	6.1	–	0.83
PBE[29]	4.2	6.0	0.51	–
BLYP	n/a	n/a	n/a	n/a
		DFT with corrections		
ACFDT-LDA[29]	3.8	5.4	1.4	–
ACFDT-PBE[29]	3.7	5.3	1.9	–
DFT-D(PW91) (Ortmann)[45]	4.2	6.0	–	0.91
SCP-DFT	3.66	5.17	2.73	6.0
SCP-DFT/QZV3P	3.70	5.24	2.38	3.9
SCP-DFT/QZV3P/2 × ATM	**3.75**	**5.31**	**2.10**	**4.5**
		ab initio calculations and benchmarks		
LMP2[85]	3.68	5.20	2.1354	2.79
CCSD(T)[80]	3.736	5.284	1.9098	2.72
Lotrich[79] (2 body[51])	3.7508[b]	5.3044	2.1709	–
Lotrich[79] (2 + 3 body[51,53])	3.7508[b]	5.3044	2.0347	–
		empirical calculations and experimental benchmarks		
LJ (effective 2 body)	**3.74**	**5.29**	**1.94**	**3.0**
experiment 1[89]	3.7508	5.3044	2.0283[c]	–
experiments 2−4[90−92]	3.70[90]	5.23[90]	2.0507[91]	2.38[92]

[a] B_0 was obtained[88] as $B_0 = (1/(9cr_{ss,\,min}))((\partial^2 E_{coh})/(\partial r_{ss}^2))(r_{ss,\,min})$, where $c = 1/\sqrt{2}$ for the fcc crystal. Note that zero-point effects are not included. "n/a" indicates that the curve is repulsive. Final results of this work are highlighted in bold font. See the text for additional details. [b] Lotrich and Szalewicz[79] presented results at the minimum experimental separation given in ref 89. [c] This value has been obtained by subtracting the zero-point effects estimated by Lotrich and Szalewicz.[79]

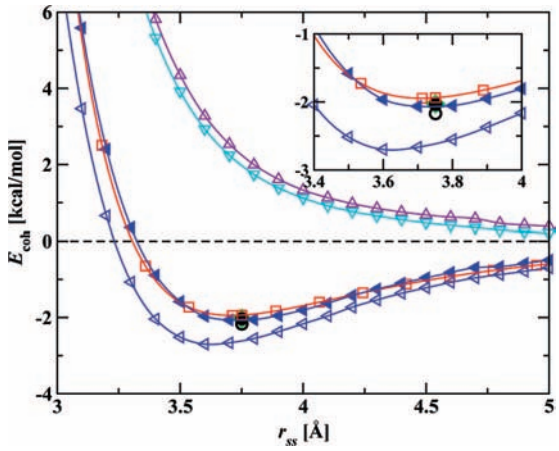

Figure 5. Cohesion energy curves (per atom) of argon fcc solid as a function of nearest-neighbor separation. Note that zero-point effects are not included. Experiment 1[89] (green diamond), Lotrich[79] (2 body[51]) (black open circle), Lotrich[79] (2 + 3 body[51,53]) (black closed circle), LJ (red squares), BLYP/QZV3P (purple up triangles), BLYP/DZVP (cyan down triangles), SCP-DFT (blue open left triangles), and SCP-DFT/QZV3P/2 × ATM (blue close left triangles). Inset shows a close-up of the minimum region. See the text for details.

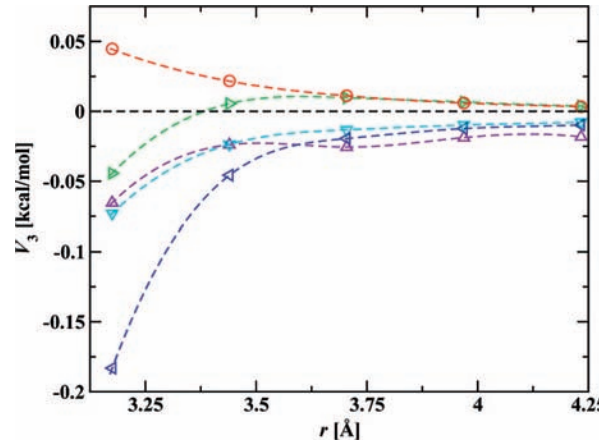

Figure 6. Three-body nonadditive interaction energies of Ar_3 in the equilateral configuration: CCSD(T)[54] (green right triangles), ATM (red circles), BLYP/QZV3P (purple up triangles), BLYP/DZVP (cyan down triangles), and SCP-DFT (blue left triangles).

the accurate benchmarks. The LJ potential also performs quite well, much better than it did for the dimer, as it was parametrized to bulk properties.

6. Conclusion

Driven by the need to perform accurate statistical mechanical sampling and chemistry in the condensed phase, we have developed an efficient correction to DFT based on linear response theory with the addition of auxiliary polarization functions to account for classical many-body polarization and a self-consistent treatment of two-body dispersion interactions. Moreover, SCP-DFT, as applied to argon, requires just two independent parameters, a_α (which itself depends on ζ_α) and I_α. They are determined by fitting to the known polarizability and a single point on the accurate dimer potential curve, respectively. With these two parameters, we are able to reproduce accurate structural, energetic, and thermodynamic quantities in all three phases of argon; a case study in weak interactions. Future work will include calculations of the vapor−liquid equilibria of argon, as well as simulations of liquid argon under high pressures. Improvements to the current theory are underway and incorporate more polarization functions, i.e., *s* and *d* functions (only the latter would be allowed to contribute to the dispersion term), as well as an environmental (or atomic charge-state) dependence of the corresponding multipole polarizability parameters a_α and a more rigorous screening function. Note that the latter will effect the charge balance in

the system. Although these extensions to the theory are important, we are confident that the formulation presented in this manuscript is sufficient to accurately describe rare gases. Future studies will focus on molecular liquids such as water where DFT in conjunction with BLYP is known to underbind the clusters. Hence, SCP-DFT should be an ideal candidate to describe the subtle interactions giving rise to the correct thermodynamics and spectra in this important and well-characterized liquid.

Acknowledgment. K.A.M. would like to acknowledge support from the Summer Research Institute at Pacific Northwest National Laboratory (PNNL). The work at the University of Minnesota is supported through research grants from the National Science Foundation (CTS-0553911 and CBET-0756641). We are grateful for the computer resources provided by the National Energy Research Scientific Computing Center, the Minnesota Supercomputing Institute. C.J.M. acknowledges computer time on NWice of the Energy Smart Data Center housed in the EMSL, a national scientific user facility sponsored by the Department of Energy's Office of Biological and Environmental Research located at Pacific Northwest National Laboratory. C.J.M. and G.K.S. would also like to gratefully acknowledge numerous conversations with Juerg Hutter, Joost VandeVondele, and Teodoro Laino. A special thanks to Teodoro Laino for helping with the implementation of the restart capability for the SCP-DFT module in CP2K. G.M. gratefully acknowledges discussions with Krzysztof Szalewicz and earlier work and discussions on weak interactions with Giacinto Scoles. G.K.S., C.J.M., and G.M. are supported by the U.S. Department of Energy's (DOE) Office of Basic Energy Sciences Chemical, Geosciences and Biosciences division. PNNL is operated by Battelle for the U.S. DOE.

References and Notes

(1) Hohenberg, P.; Kohn, W. *Phys. Rev.* **1964**, *136*, B864.
(2) Kohn, W.; Sham, L. J. *Phys. Rev.* **1965**, *140*, A1133.
(3) Perdew, J. P.; Ruzsinszky, A.; Tao, J.; Staroverov, V. N.; Scuseria, G. E.; Csonka, G. I. *J. Chem. Phys.* **2005**, *123*, 062201.
(4) Tao, J. M.; Perdew, J. P.; Staroverov, V. N.; Scuseria, G. E. *Phys. Rev. Lett.* **2003**, *91*, 146401.
(5) Wu, X.; Vargas, M. C.; Nayak, S.; Lotrich, V.; Scoles, G. *J. Chem. Phys.* **2001**, *115*, 8748.
(6) Tsuzuki, S.; Lüthi, H. P. *J. Chem. Phys.* **2001**, *114*, 3949.
(7) Kuo, I.-F. W.; Mundy, C. J.; McGrath, M. J.; Siepmann, J. I.; VandeVondele, J.; Sprik, M.; Hutter, J.; Chen, B.; Klein, M. L.; Mohamed, F.; Krack, M.; Parrinello, M. *J. Phys. Chem. B* **2004**, *108*, 12990.
(8) Kuo, I.-F. W.; Mundy, C. J.; McGrath, M. J.; Siepmann, J. I. *J. Phys. Chem. C* **2008**, *112*, 15412.
(9) Allesch, M.; Lightstone, F. C.; Schwegler, E.; Galli, G. *J. Chem. Phys.* **2008**, *128*, 014501.
(10) Cicero, G.; Grossman, J. C.; Schwegler, E.; Gygi, F.; Galli, G. *J. Am. Chem. Soc.* **2008**, *130*, 1871.
(11) Sharma, M.; Resta, R.; Car, R. *Phys. Rev. Lett.* **2007**, *98*, 247401.
(12) McGrath, M. J.; Siepmann, J. I.; Kuo, I.-F. W.; Mundy, C. J. *Mol. Phys.* **2006**, *104*, 3619.
(13) McGrath, M. J.; Siepmann, J. I.; Kuo, I.-F. W.; Mundy, C. J. *J. Phys. Chem. A* **2006**, *110*, 640.
(14) Chałasiński, G.; Szcześniak, M. M. *Chem. Rev.* **1994**, *94*, 1723.
(15) Bukowski, R.; Szalewicz, K.; Groenenboom, G. C.; van der Avoird, A. *Science* **2007**, *315*, 1249.
(16) Jeziorski, B.; Moszynski, R.; Szalewicz, K. *Chem. Rev.* **1994**, *94*, 1887.
(17) Misquitta, A. J.; Jeziorski, B.; Szalewicz, K. *Phys. Rev. Lett.* **2003**, *91*, 033201.
(18) Hesselmann, A.; Jansen, G. *Phys. Rev. Lett.* **2003**, *367*, 778.
(19) Podeszwa, R.; Rice, B. M.; Szalewicz, K. *Phys. Rev. Lett.* **2008**, *101*, 115503.
(20) Grimme, S.; Antony, J.; Schwabe, T.; Mück-Lichtenfeld, C. *Org. Biomol. Chem.* **2007**, *5*, 741.
(21) Hamprecht, F. A.; Cohen, A. J.; Tozer, D. J.; Handy, N. C. *J. Chem. Phys.* **1998**, *109*, 6264.
(22) Boese, A. D.; Doltsinis, N. L.; Handy, N. C.; Sprik, M. *J. Chem. Phys.* **2000**, *112*, 1670.
(23) Becke, A. D. *J. Chem. Phys.* **1997**, *107*, 8554.
(24) Zhao, Y.; Truhlar, D. G. *Theor. Chem. Acc.* **2008**, *120*, 215.
(25) von Lilienfeld, O. A.; Tavernelli, I.; Rothlisberger, U.; Sebastiani, D. *Phys. Rev. Lett.* **2004**, *114*, 153004.
(26) von Lilienfeld, O. A.; Tavernelli, I.; Rothlisberger, U.; Sebastiani, D. *Phys. Rev. B* **2004**, *71*, 195119.
(27) Lin, I.-C.; Rothlisberger, U. *Phys. Chem. Chem. Phys.* **2008**, *114*, 2730.
(28) Dion, M.; Rydberg, H.; Schröder, E.; Langreth, D. C.; Lundqvist, B. I. *Phys. Rev. Lett.* **2004**, *92*, 246401.
(29) Harl, J.; Kresse, G. *Phys. Rev. B* **2008**, *77*, 045136.
(30) Podeszwa, R.; Szalewicz, K. *Chem. Phys. Lett.* **2005**, *412*, 412.
(31) Douketis, C.; Scoles, G.; Marchetti, S.; Zen, M.; Thakkar, A. J. *J. Chem. Phys.* **1982**, *76*, 3057.
(32) Murdachaew, G.; de Gironcoli, S.; Scoles, G. *J. Phys. Chem. A* **2008**, *112*, 9993.
(33) Perdew, J. P.; Burke, K.; Ernzerhof, M. *Phys. Rev. Lett.* **1996**, *77*, 3865.
(34) Zhang, Y.; Yang, W. *Phys. Rev. Lett.* **1998**, *80*, 890.
(35) Hammer, B.; Hansen, L. B.; Nørskov, J. K. *Phys. Rev. B* **1999**, *59*, 7413.
(36) Becke, A. D. *Phys. Rev. A* **1988**, *38*, 3098.
(37) Lee, C.; Yang, W.; Parr, R. G. *Phys. Rev. B* **1988**, *37*, 785.
(38) Becke, A. D. *J. Chem. Phys.* **1993**, *98*, 5648.
(39) Perdew, J. P.; Chevary, J. A.; Vosko, S. H.; Jackson, K. A.; Pederson, M. R.; Fiolhais, C. *Phys. Rev. B* **1992**, *46*, 6671.
(40) Frauenheim, T.; Seifert, G.; Elstner, M.; Hajnal, Z.; Jungnickel, G.; Porezag, D.; Suhai, S.; Scholz, R. *Phys. Status Solidi B* **2000**, *217*, 41.
(41) Elstner, M.; Hobza, P.; Frauenheim, T.; Suhai, S.; Kaxiras, E. *J. Chem. Phys.* **2001**, *114*, 5149.
(42) Wu, Q.; Yang, W. *J. Chem. Phys.* **2002**, *116*, 515.
(43) Grimme, S. *J. Comput. Chem.* **2004**, *25*, 1463.
(44) Zimmerli, U.; Parrinello, M.; Koumoutsakos, P. *J. Chem. Phys.* **2004**, *120*, 2693.
(45) Ortmann, F.; Bechstedt, F.; Schmidt, W. G. *Phys. Rev. B* **2006**, *73*, 205101.
(46) Silvestrelli, P. L. *Phys. Rev. Lett.* **2008**, *100*, 053002.
(47) Becke, A. D.; Johnson, E. R. *J. Chem. Phys.* **2006**, *124*, 014104.
(48) Chang, D. T.; Schenter, G. K.; Garrett, B. C. *J. Chem. Phys.* **2008**, *128*, 164111.
(49) Tabacchi, G.; Mundy, C. J.; Hutter, J.; Parrinello, M. *J. Chem. Phys.* **2002**, *117*, 1416.
(50) Tabacchi, G.; Hutter, J.; Mundy, C. J. *J. Chem. Phys.* **2005**, *123*, 074108.
(51) Aziz, R. A. *J. Chem. Phys.* **1993**, *99*, 4518.
(52) Patkowski, K.; Murdachaew, G.; Fou, C. M.; Szalewicz, K. *Mol. Phys.* **2005**, *103*, 2031.
(53) Lotrich, V. F.; Szalewicz, K. *J. Chem. Phys.* **1997**, *106*, 9688.
(54) Podeszwa, R.; Szalewicz, K. *J. Chem. Phys.* **2007**, *126*, 194101.
(55) The CP2K developers group; http://cp2k.berlios.de/, 2008.
(56) Longuet-Higgins, H. C. *Discuss. Faraday Soc.* **1965**, *40*, 7.
(57) VandeVondele, J.; Krack, M.; Mohamed, F.; Parrinello, M.; Chassaing, T.; Hutter, J. *Comput. Phys. Commun.* **2005**, *167*, 103.
(58) Goedecker, S.; Teter, M.; Hutter, J. *Phys. Rev. B* **1996**, *54*, 1703.
(59) Hartwigsen, C.; Goedecker, S.; Hutter, J. *Phys. Rev. B* **1998**, *58*, 3641.
(60) Krack, M. *Theor. Chem. Acc.* **2005**, *114*, 145.
(61) Martyna, G. J.; Tuckerman, M. E. *J. Chem. Phys.* **1999**, *110*, 2810.
(62) In *CRC Handbook of Chemistry and Physics, Internet Version*, 87th ed.; Lide, D. R., Ed.; Taylor and Francis: Boca Raton, FL, 2007.
(63) Potoff, J. J.; Panagiotopoulos, A. Z. *J. Chem. Phys.* **1998**, *109*, 10914.
(64) Michels, A.; Levelt, J. M.; de Graaff, W. *Physica* **1958**, *24*, 659.
(65) Siepmann, J. I. In *Forum 2000: Fluid Properties for New Technologies, Connecting Virtual Design with Physical Reality*; Rainwater, J. C., Friend, D. G., Hanley, H. J. M., Harvey, A. H., Holcomb, C. D., Laesecke, A., Magee, J. W., Muzny, C., Eds.; Vol. NIST Special Publication 975; NIST: Boulder, CO, 2001; p 110.
(66) Nosé, S. *J. Chem. Phys.* **1984**, *81*, 511.
(67) Nosé, S. *Mol. Phys.* **1984**, *52*, 255.
(68) Hoover, W. G. *Phys. Rev. A* **1986**, *34*, 2499.
(69) Nosé, S. *Mol. Phys.* **1986**, *57*, 187.
(70) Hutter, J. V. J. *J. Chem. Phys.* **2003**, *118*, 4365.
(71) Lupinetti, C.; Thakkar, A. *J. Chem. Phys.* **2005**, *122*, 044301.
(72) Kislyakov, I. M. *Opt. Spectrosc.* **1999**, *87*, 357.
(73) McQuarrie, D. A. *Statistical Mechanics*; University Science Books: New York, 2000.
(74) Dardi, P. S.; Dahler, J. S. *Theor. Chim. Acta* **1992**, *82*, 117.
(75) Dymond, J. H.; Smith, E. B. *The Virial Coefficients of Pure Gases and Mixtures: A Critical Compilation*; Oxford University Press: Oxford, 1980.

(76) Naumkin, F. Y.; Wales, D. J. *Mol. Phys.* **1999**, *96*, 1295.
(77) Wales, D. J.; Doye, J. P. K.; Dullweber, A.; Hodges, M. P.; Naumkin, F. Y.; Calvo, F. ; Hernández-Rojas, J.; Middleton, T. F. The Cambridge Cluster Database;http://www-wales.ch.cam.ac.uk/CCD.html.
(78) Bukowski, R.; Szalewicz, K. *J. Chem. Phys.* **2001**, *114*, 9518.
(79) Lotrich, V. F.; Szalewicz, K. *Phys. Rev. Lett.* **1997**, *79*, 1301.
(80) Rościszewski, K.; Paulus, B.; Fulde, P.; Stoll, H. *Phys. Rev. B* **1999**, *60*, 7905.
(81) Axilrod, B. M.; Teller, E. *J. Chem. Phys.* **1943**, *11*, 299.
(82) Muto, Y. *Proc. Phys. Math. Soc. Jpn.* **1943**, *17*, 629.
(83) Thakkar, A. J.; Hettema, H.; Wormer, P. E. S. *J. Chem. Phys.* **1992**, *97*, 3252.
(84) Tkatchenko, A.; von Lilienfeld, O. A. *Phys. Rev. B* **2008**, *78*, 045116.
(85) Casassa, S.; Halo, M.; Maschio, L. *J. Phys.: Conf. Ser.* **2008**, *117*, 012007.
(86) Herman, P. R.; LaRocque, P. E.; Stoicheff, B. P. *J. Chem. Phys.* **1988**, *89*, 4535.
(87) Bruch, L. W.; Diehl, R. D.; Venables, J. A. *Rev. Mod. Phys.* **2007**, *79*, 1381.
(88) Schwerdtfeger, P.; Gaston, N.; Krawczyk, R. P.; Tonner, R.; Moyano, G. E. *Phys. Rev. B* **2006**, *73*, 064112.
(89) Tessier, C.; Terlain, A.; Larher, Y. *Physica (Amsterdam)* **1982**, *113A*, 286.
(90) Peterson, O. G.; Batchelder, D. N.; Simmons, R. O. *Phys. Rev.* **1966**, *150*, 703.
(91) Schwalbe, L. A.; Crawford, R. K.; Chen, H. H.; Aziz, R. A. *J. Chem. Phys.* **1977**, *66*, 4493.
(92) Gewurtz, S.; Stoicheff, P. *Phys. Rev. B* **1974**, *10*, 3487.
(93) Yarnell, J. L.; Katz, M. J.; Wenzel, R. G.; Koenig, S. H *Phys. Rev. A* **1973**, *7*, 2130.

JP808767Y